Supporting information

Mesoporous organosilicas with thiol functionalized pores: Multifunctional dendrimers as sacrificial building block and template

Mathilde LAIRD*, Niklas HERRMANN, Carole CARCEL, Philippe TRENS, Erwan OLIVIERO, Guillaume TOQUER, Rozenn LE PARC, Jean-Louis BANTIGNIES, John R. BARTLETT* and Michel WONG CHI MAN*

S1. Table of Contents

S2. Experimental

S2.1 General route to acetylenic PAMAM dendrimers

PAMAM S-S propargyl G3 dendrimer

The reaction was performed with (propargyloxyethyl)(ethylacrylate)disulfide (4.1 mmol, 1.0 g, 2 eq/NH) in dry methanol (0.2 mL) and PAMAM-$(NH_2)_{32}$ G3 (31.7 µmol, 219 mg, 1 eq) in dry methanol (0.8 mL). PAMAM G3 being commercially available as a 20 wt% in methanol, it was evaporated and re-dissolved in the required quantity of methanol for the reaction. The crude reaction product was purified by successive washing with pentane. A viscous yellow oil was obtained. **Yield:** 91% (652 mg, 28.8 µmol) **^{1}H NMR (400 MHz, $CDCl_3$, δ, ppm):** 4.34 (t, 128H, J=6.6 Hz, S-CH_2-**CH_2**-O-(C=O)), 4.20 (d, 128H, J=2.2 Hz, HC≡C-**CH_2**-O), 3.91 (m, **PAMAM branches**), 3.79 (t, 128H, J=6.4 Hz, CH_2-O-**CH_2**-CH_2-S), 3.67 (s, 4H, **PAMAM core**), 3.26 (m, **PAMAM branches**), 2.93 (m, S-**CH_2**-CH_2-O-(C=O) & CH_2-O-CH_2-**CH_2**-S & **PAMAM branches**), 2.79 (m, **PAMAM branches** & N-CH_2-**CH_2**-(C=O)), 2.56 (m, **PAMAM branches**), 2.47 (m, **PAMAM branches** & N-**CH_2**-CH_2-(C=O) & **HC**≡C-CH_2-O), 2.36 (t, 8H, J=5.6 Hz, **PAMAM branch**) **^{13}C NMR (100 MHz, $CDCl_3$, δ, ppm):** 173.15, 172.56, 172.45, 79.49, 75.24, 68.11, 67.99, 62.49, 60.22, 58.24, 52.84, 52.42, 51.82, 49.83, 49.16, 41.38, 38.32, 37.30, 33.76, 33.76 **IR (ν, cm^{-1}):** 3282 (≡C-H), 1729 (C=O), 1643 (amide I), 1533 (amide II) **MALDI-MAS:** An appropriate desorption matrix could not be identified.

S2.2 General procedure for obtaining triethoxysilylated dendrimers via click reactions

PAMAM-G3 S-S triethoxysilane dendrimer

The reaction was carried out with PAMAM-G3 S-S (R-C≡CH)$_{64}$ (3.1 µmol, 70 mg, 1 eq) in dry DCM (1.3 mL), bis-(triethoxysilylpropyl)aminoethenylazide (198 µmol, 97.8 mg, 1 eq/alkyne) in dry DCM (1.3 mL) and a solution of dry CuI (9.9 µmol, 1.9 mg, 5 mol%) and distilled DIPEA (397 µmol, 70 µL, 2 eq/alkyne) in dry DCM (1.3 mL). The reaction was held for 10 min under microwave irradiation at 60 °C. **Yield:** quantitative ($C_{2222}H_{4448}N_{378}O_{636}S_{128}Si_{128}$, 163.0 mg, 3.0 µmol) **^{1}H NMR (400 MHz, $CDCl_3$, δ, ppm):** 7.66 (s, 64H, **$H_{triazole}$**), 4.65 (s, 128H, O-**CH_2**-$C_{triazole}$), 4.38 (t, 128H, $N_{triazole}$-**CH_2**-CH_2-N), 4.30 (t, PAMAM branches), 3.80 (m, CH_2-O-**CH_2**-CH_2-S & O-**CH_2**-CH_3 & S-CH_2-**CH_2**-O-(C=O)), 3.65 (s, 4H, **PAMAM core**), 3.5 (m, 8H, **PAMAM branch**), 2.90 (m, 48H, S-**CH_2**-CH_2-O-(C=O) & CH_2-O-CH_2-**CH_2**-S & $N_{triazole}$-CH_2-**CH_2**-N), 2.78 (t, N-CH_2-**CH_2**-(C=O)), 2.65 (m, **PAMAM branches**), 2.56 (t, **PAMAM branches**), 2.48 (m, **PAMAM branch** & N-**CH_2**-CH_2-(C=O) & N-**CH_2**-CH_2-CH_2-Si), 2.33 (t, **PAMAM branch**), 1.50 (m, 256H, CH_2-**CH_2**-CH_2-Si), 1.21 (m, 256H, CH_3-**CH_2**-O-Si), 0.54 (m, 256H, CH_2-CH_2-**CH_2**-Si) **^{13}C NMR (100 MHz, $CDCl_3$, δ, ppm):** 172.40, 144.46 (triazole), 123.52, 68.64, 68.41, 64.42, 62.54, 60.38, 58.43 (ethoxy), 57.10, 54.36, 48.97, 41.32, 38.74, 20.44, 18.43 (ethoxy), 7.91 **^{29}Si NMR (80 MHz, $CDCl_3$, δ, ppm):** -45.18 **IR (ν, cm^{-1}):** 1734 (C=O), 1650 (amide I), 1546 (amide II), 1072 (C-O) **MALDI-MS:** An appropriate desorption matrix could not be identified.

S2.3 Preparation of gels

Synthesis of PAMAM-G3 gel and DTT treatment

In a flame-dried Schlenk flask, the solution of PAMAM-G3-Si$(OEt)_3$ (13.2 µmol, 719 mg, 1 eq) resulting from the click reaction was dried under vacuum. The resulting greenish PAMAM-G3-Si$(OEt)_3$ viscous oil was then dissolved in dry THF (1.2 mL) under nitrogen. Water (16.9 mmol, 300 µL, 10 eq/Si) was added, followed by TBAF (1 M in THF) (34 µmol, 35 µL, 0.02 eq/Si). The mixture formed a gel in a few minutes. The material was then aged for three days. After aging, the green solid was crushed. The powder was split into two parts. One third was washed three times with water and three times with acetone then dried under vacuum overnight to obtain a green powder. **^{13}C NMR (75 MHz, CP-MAS, δ, ppm):** 172.2 (amide), 144.1 (triazole), 123.8 (triazole), 51.6-10.0 (cluster) **^{29}Si**

NMR (60 MHz, CP-MAS, δ, ppm): -65.6 (T^3_{PAMAM}) **IR (ν, cm^{-1}):** 1729 (C=O), 1646 (amide I), 1544 (amide II), 1192-1013 (Si-O-Si).

The remaining two thirds of the wet powder were suspended in water (10 mL). In order to outgas the solvent, five freeze/pump/thaw cycles were performed. An excess of DTT (1.7 mmol, 261 mg, 1 eq/max quantity of S-S) was then added under an inert atmosphere to cleave the disulfide bonds. The reaction was stirred at room temperature for 3 days. After cleavage, the solid was washed three times with water, three times with acetone and dried under vacuum overnight. **^{13}C NMR (75 MHz, CP-MAS, δ, ppm):** 171.9 (amide), 144.0 (triazole), 123.7 (triazole), 50.7-10.2 (cluster) **^{29}Si NMR (60 MHz, CP-MAS, δ, ppm):** -59.7 (T^2_{PAMAM}), -65.7 (T^3_{PAMAM}) **IR (ν, cm^{-1}):** 1732 (C=O), 1649 (amide I), 1192-1013 (Si-O-Si).

Synthesis of PAMAM-G3/BTEB gel and DTT treatment

In a flame-dried Schlenk flask, the solution of PAMAM-G3-Si(OEt)$_3$ (3.1 µmol, 168 mg, 1 eq) was mixed with BTEB (1.2 mmol, 480 µL, 48 eq). The mixture was dried under vacuum to obtain a PAMAM-G3-Si(OEt)$_3$ solution in BTEB. The resulting mixture was dissolved in dry THF (1.8 mL) under nitrogen. Water (2.8 mmol, 50 µL, 1 eq/Si) was added followed by TBAF (1 M in THF) (55 µmol TBAF, 55 µL solution, 0.02 eq/Si). The mixture gelled within a few minutes. The material was then aged for 3 days. After aging, the light green solid was crushed. One third was washed three times with water and three times with acetone then dried under vacuum overnight to obtain a light green powder. **^{13}C NMR (75 MHz, CP-MAS, δ, ppm):** 173.5 (amide), 144.3 (triazole), 133.7 (aromatic BTEB), 69.1-11.1 (cluster) **^{29}Si NMR (60 MHz, CP-MAS, δ, ppm):** -62.2 (T^1_{BTEB}), -70.6 (T^2_{BTEB}), -78.9 (T^3_{BTEB}) **IR (ν, cm^{-1}):** 1722 (C=O), 1146-1016 (Si-O-Si).

The remaining two third of the wet powder was used for DTT cleavage and suspended in water (10 mL). In order to outgas the solvent, five freeze/pump/thaw cycles were performed prior to addition of the powder. An excess of DTT (396 µmol, 61.0 mg, 1 eq/max quantity of S-S) was then added under an inert atmosphere. The reaction was stirred at room temperature for three days. After cleavage, the solid was washed three times with water, three times with acetone and dried under vacuum overnight. **^{13}C NMR (75 MHz, CP-MAS, δ, ppm):** 174.7 (amide), 144.2 (triazole), 133.5 (aromatic BTEB), 69.8-9.2 (cluster) **^{29}Si NMR (60 MHz, CP-MAS, δ, ppm):** -61.6 (T^1_{BTEB}), -70.4 (T^2_{BTEB}), -78.9 (T^3_{BTEB}) **IR (ν, cm^{-1}):** 1146-1016 (Si-O-Si).

S2.4 General procedure for gold impregnation

A solution of $NaAuCl_4 \cdot 2H_2O$ (176 µmol, 70.0 mg) in pure water (100 mL) and a solution of $NaBH_4$ (870 µmol, 33.0 mg) in pure water (100 mL) were prepared. A sample of the PAMAM/BTEB gel (100 mg) was suspended in 62.5 mL of the gold solution (110 µmol Au, 1.6 eq compared to the maximum thiol content) and stirred for 2.5 hours. The resulting solid was then washed three times with water by centrifugation and then resuspended in 68 mL of water. $NaBH_4$ solution (55 µmol, 6.3 mL, 0.8 eq compared to the maximum thiol content) was added and the suspension was stirred for 30 min. The resulting solid was washed three times with ethanol. The gold impregnation/$NaBH_4$ treatment was then repeated, and the resulting solid was dried at ambient temperature.

The same procedure was used for the impregnation of the PMO sample with the following adapted reactant proportions: PMO after DTT treatment (45.6 mg) in the $NaAuCl_4$-solution (8.1 µmol, 4.6 mL, 1.6 eq compared to the maximum thiol content). Re-dispersion in pure water (5 mL), reduction with $NaBH_4$-solution (4.1 µmol, 500 µL, 0.8 eq compared to the maximum thiol content).

S2.5 Characterisation

Thermogravimetric analyses (TGA) were carried out between 25 and 800 °C, on a TA Instruments Q50 apparatus, with a heating rate of 10 °C.min^{-1} under an air flow of 60 mL.min^{-1}.

S3. Results and Discussion

S3.1 Dendrimer synthesis

The approach used to construct the multifunctional acetylenic linker is illustrated in **Scheme 1**. The first part of the reaction involves the mono-substitution of propargyl bromide on a single terminal hydroxyl function of the bis(hydroxyethyl)disulfide, as described elsewhere.[1-2] The pure monopropargyl disulfide precursor is then functionalized on the remaining hydroxyl group by an acrylate group via a nucleophilic acyl substitution. The ^{1}H NMR spectrum of the linker (**Figure S1**) exhibits signals at 6.43, 6.12 and 5.85 ppm, which are consistent with the presence of the acrylate moiety. In addition, the signal arising from the CH associated with the propargyl moiety is observed at 2.45 ppm, together with that of the proximal CH_2 group at 4.19 ppm. The signals at 4.42, 3.79, 2.98 and 2.92 ppm are attributed to the four CH_2 groups located between the S-S and the O-C=O. The structure was also confirmed by ^{13}C NMR spectroscopy, mass spectrometry and IR.

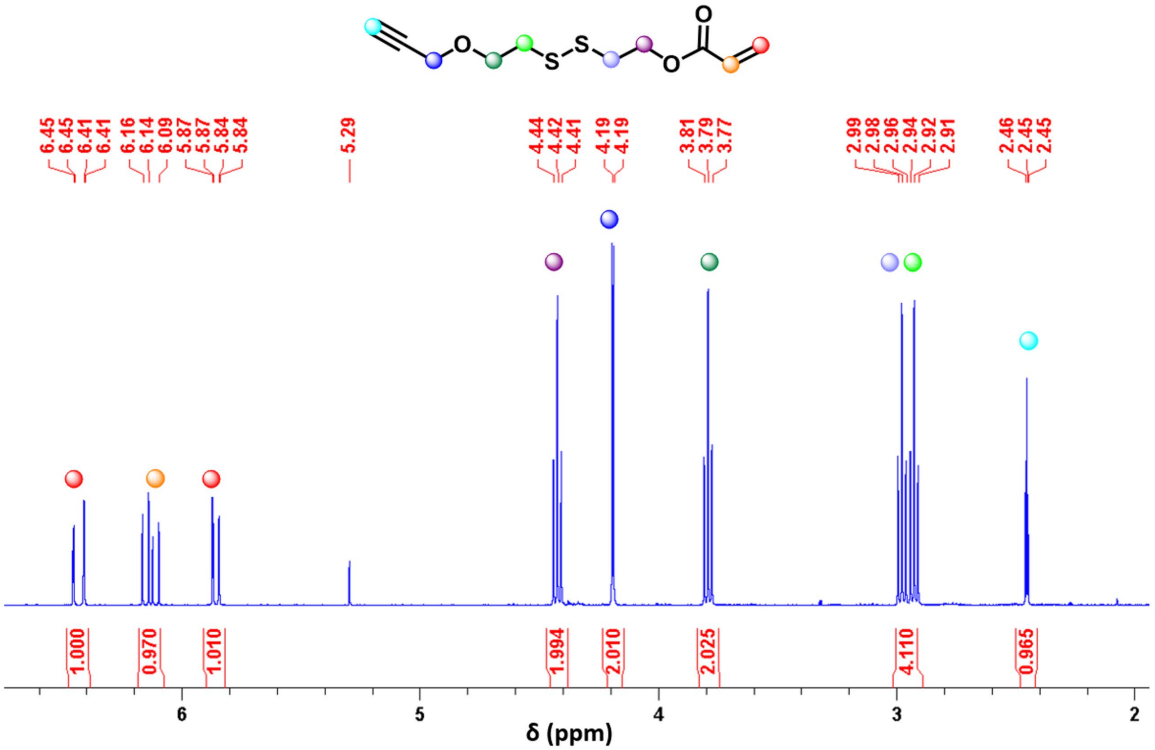

Figure S1. ^{1}H NMR spectrum of the acetylenic S-S linker ($CDCl_3$)

The linker was subsequently grafted onto the PAMAM dendrimers via a Michael addition (informed by the protocols used for the PAMAM dendrimer synthesis[3]), as illustrated in **Scheme 1** (Main Text) for the particular case of the G0 system. This approach enables the dendrimer to be grown by the equivalent of half a generation, which doubles the number of active groups compared to the full starting generation. Interestingly, the alumina-pad purification step used for the PAMAM-G0 dendrimer could not be used for the PAMAM-G3 dendrimer, presumably because of the higher quantity of amide groups which leads to stronger interactions between the product and the stationary phase. The PAMAM-G3 dendrimer was consequently purified by consecutive washing with pentane, taking advantage of the poor solubility of the G3 dendrimer in the latter. **Figures S2A** and **S2B** present the ^{1}H NMR spectra of the acetylenic PAMAM-G0 and -G3, respectively, together with the corresponding signal attributions. The signal arising from the CH_2 in the α-position of the propargyl group is visible at 4.20 ppm in both spectra. The chemical shifts and integrated intensities of all other signals are consistent with the target compounds. IR spectroscopy (**Figures S3** and **S4**) also confirmed

the formation of the acetylenic dendrimer. Although the region from 3100-3500 cm^{-1} consists of a complex series of superimposed bands arising from ν(OH) of water, together with broad Amide A and B bands associated with H-bonding organization (see discussion below), the region is clearly dominated by the characteristic alkyne ≡C-H stretching mode at 3287 cm^{-1}.

The silylated groups were grafted onto the acetylenic PAMAM dendrimer by a Huisgen CuAAC cycloaddition in the presence of copper iodide as a catalyst (**Scheme 1b,** Main Text). Key features of this reaction include quantitative yields, mild reaction conditions and regioselectivity ensured by the copper catalyst.[4] Bis-(triethoxysilylpropyl)aminoethenylazide was selected as the silylated reactant, to further increase the silyl group density on the periphery of the molecule. This ensures that a more robust silica network is obtained following sol-gel hydrolysis and condensation, with the quantity of triethoxysilyl functions being twice that of the acetylenic moieties. Considering the two steps of the synthesis outlined in **Scheme 1b** (Main Text), the number of active functions is increased four-fold compared to the initial PAMAM compound. A highly silylated dendrimer is thus obtained, with 16 and 128 triethoxysilyl functions for the G0 and G3 dendrimer, respectively. Stoichiometric amounts of azide reactant were used in order to avoid the need for purification of these hydrolysis-sensitive molecules. As the dendrimer can be sensitive to heat,[5] an adapted protocol was employed using microwave heating[6] and the temperature was limited to 60 °C. The reaction product was successfully obtained, as evidenced by the disappearance of the ^{1}H NMR signal of the CH_2 in the α-position of the acetylenic function at 4.19 ppm (**Figure S2**), and the presence of the signal arising from the triazole aromatic proton at 7.67 (G0) and 7.66 (G3) ppm (**Figure S5**). In addition, the signals associated with the triethoxysilyl groups for the G0 compound are visible at 1.19 and 3.76 ppm as well as those arising from the CH_2 of the propyl and ethyl groups (0.53, 1.45, 2.43, 2.88 and 4.35 ppm). The corresponding signals are also evident in the spectrum of the silylated G3 molecule. No traces of the azide precursor were evident in either case (**Figure S5**). The successful functionalization is also supported by the disappearance of the acetylenic ≡C-H mode at 3287 cm^{-1} (**Figures S3** and **S4**), with the remaining bands resulting from non-homogeneous H-bonded amide A and B vibrations (see discussion below).

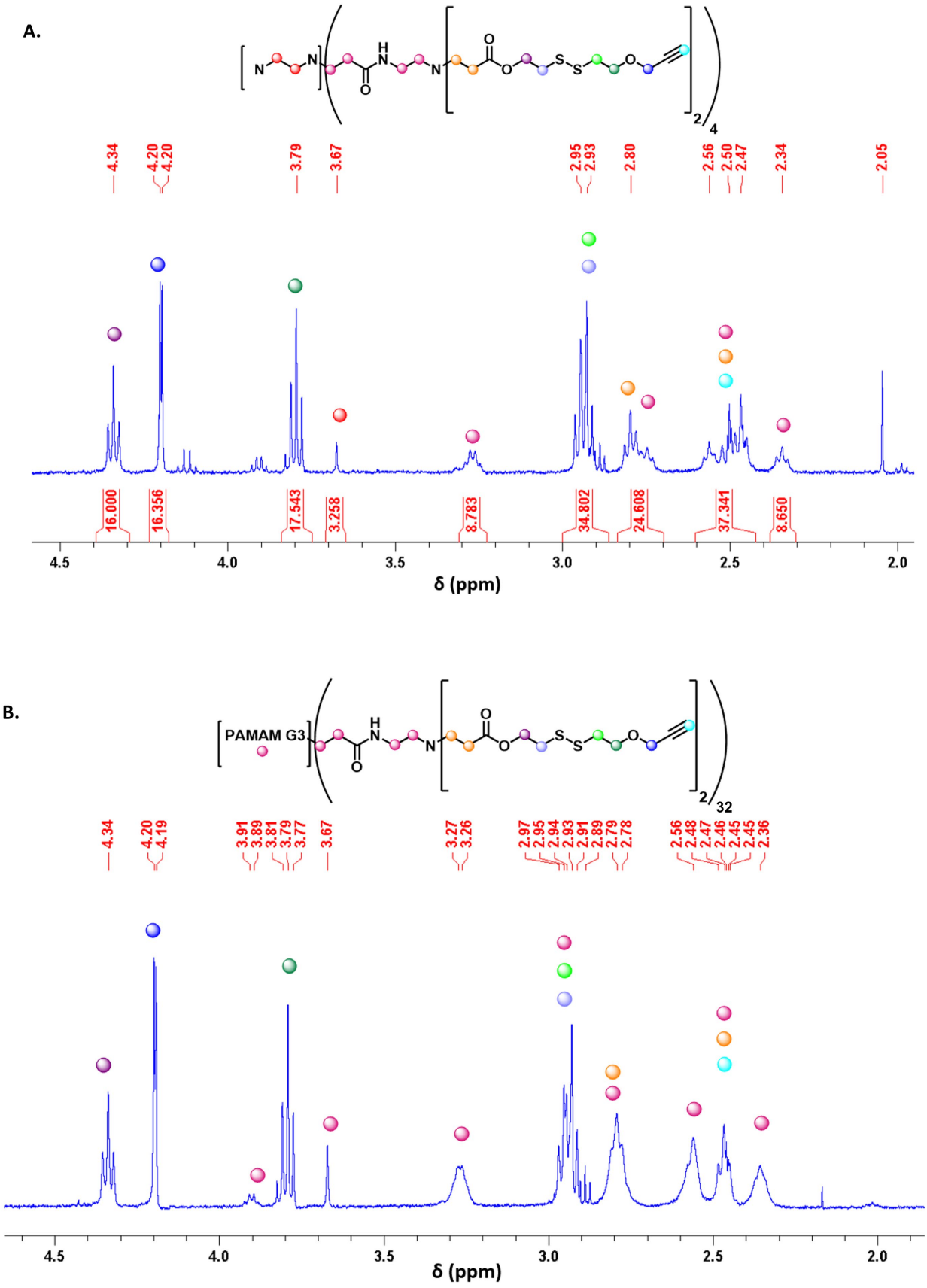

Figure S2. ^{1}H NMR spectrum of the acetylenic PAMAM-G0 (A) and -G3 (B) in $CDCl_3$

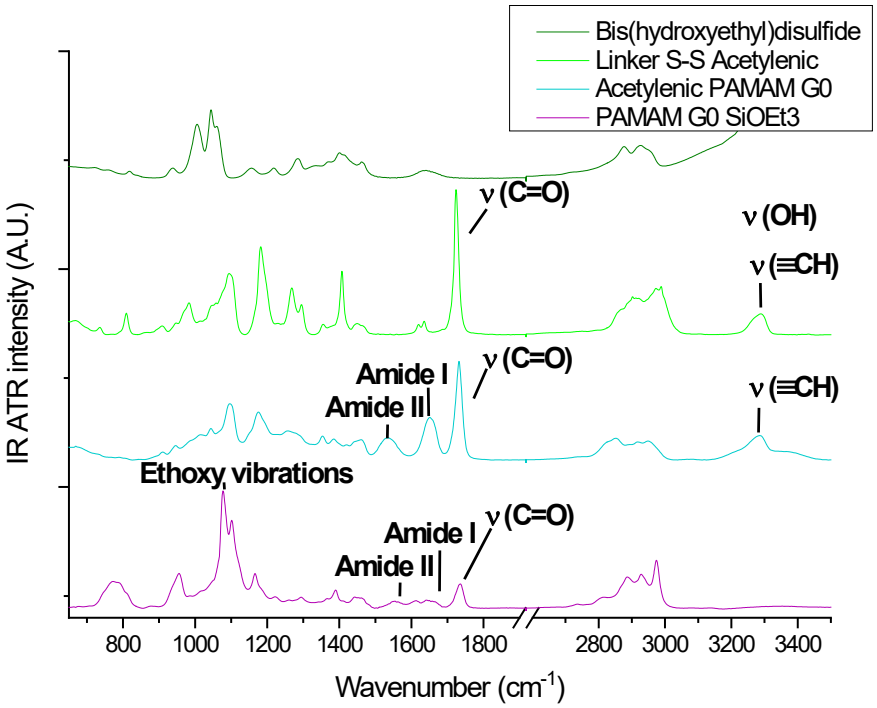

Figure S3. Infrared spectra of PAMAM-G0-Si(OEt)$_3$ and its precursors in the range 400 to 3500 cm^{-1}

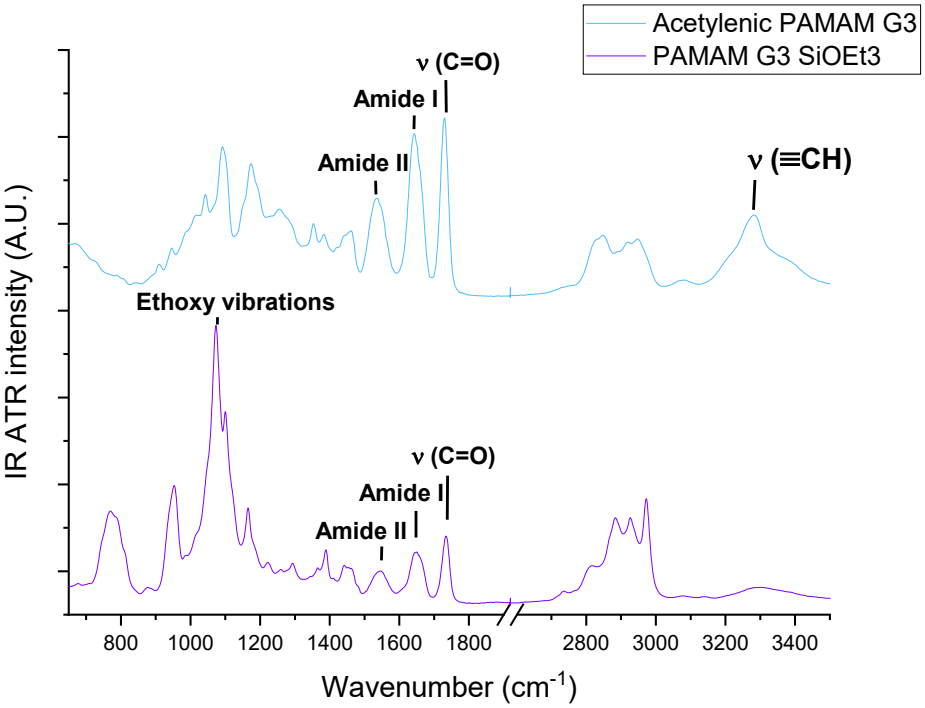

Figure S4. Infrared spectra of PAMAM-G3-Si(OEt)$_3$ and the acetylenic PAMAM-G3 in the range 650 to 3500 cm^{-1}

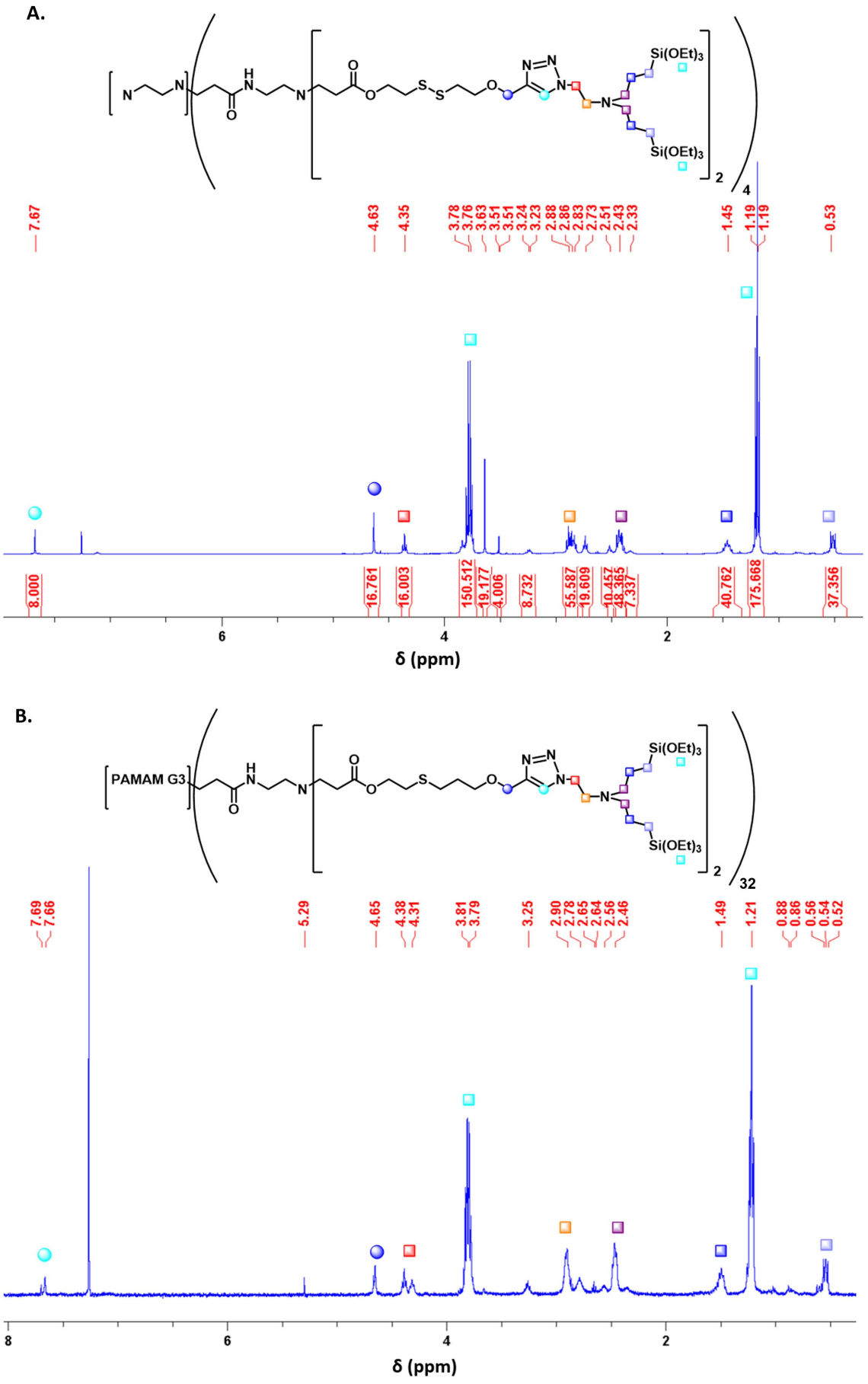

Figure S5. ^{1}H NMR spectrum of the PAMAM-$Si(OEt)_3$ A. G0 B. G3 in $CDCl_3$

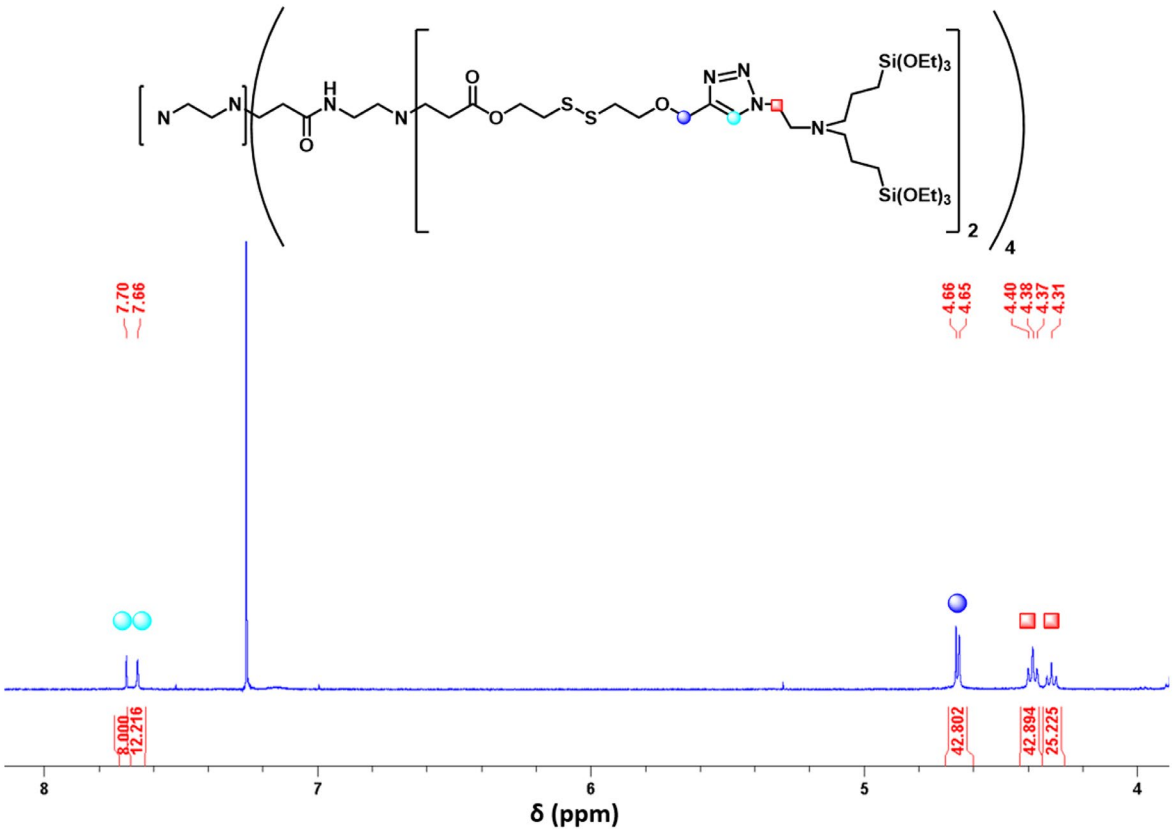

Figure S6. Expanded view of the ^{1}H NMR signals from the two different conformations of the branches of PAMAM-G0 Si(OEt)$_3$ ($CDCl_3$)

Intriguingly, more than one spectral signature was often observed via ^{1}H NMR spectroscopy for the silylated G0 compound, as shown in **Figure S6**, despite rigorous experimental protocols to ensure reproducibility. In particular, two sets of signals arising from the CH group in the triazole ring (7.66 and 7.70 ppm) and the CH_2 group located between the triazole ring and ether oxygen (4.65 and 4.66 ppm) were observed on several occasions, together with two sets of triplets at 4.39 and 4.34 ppm related to the CH_2 in the α-position of the triazole. In all three cases, only a single set of signals is expected for the target compound. This might be explained either by the presence of two regioisomers or multiple conformers. The possible formation of regioisomers is unlikely, as the copper-catalyzed azide-alkyne Huisgen cycloaddition is well-known to render a single isomer.[7] However, different conformers have been previously described in the case of PAMAM dendrimers.[8-9] Indeed, to lower peripheral steric hindrance, the branches can back-fold to fill the voids within the inner region of the dendrimer, although H-bonding, π-π interactions, and electrostatic repulsions in the periphery can prevent such back-folding.[10] Nevertheless, in our model, such interactions are less likely, and back-folding is thus possible. The presence of two different environments around the branches could explain signals arising from both back-folded and extended branches. The interpenetration by the branches of a dendrimer into the core of another dendrimer to form dendrimer "oligomers" is also possible. Different NMR solvents were used to try to relieve the constraint of the back-folding, although no significant differences were observed in the spectra with changing solvent. Additional simple energy-minimization modelling studies using Chem 3D software to approximate the steric energy in extended and backfolded dendrimer configurations were undertaken to study the possibility of back-folding. Although such modelling studies have a number of intrinsic limitations (such as the neglect of solute-solvent interactions), they suggest that the steric energy in the back-folded

configuration is lower by more than one hundred kJ/mol than in the expanded structure. Hence, despite the approximations involved, the results are consistent with the potential formation of back-folded branches. Different solvents were also used in an attempt to avoid conformer formation during the synthesis, including THF, methanol, mixed methanol/THF, and dichloromethane. Although, a single set of signals were obtained in some cases, it appears that extremely subtle changes in experimental conditions can promote or impede back-folding/interpenetration. However, we note that the results obtained are entirely consistent with the formation of the target compound shown in **Scheme 1b** (Main Text).

Consequently, to facilitate the treatment of the reaction product, dichloromethane (DCM) was finally chosen as a solvent for the Click CuAAC reaction. Indeed, we note that dendrimers generally swell with solvent, with the latter typically remaining entrapped in the dendrimers.

S3.2 Gel synthesis and inner dendrimer cleavage

Solid state NMR characterization

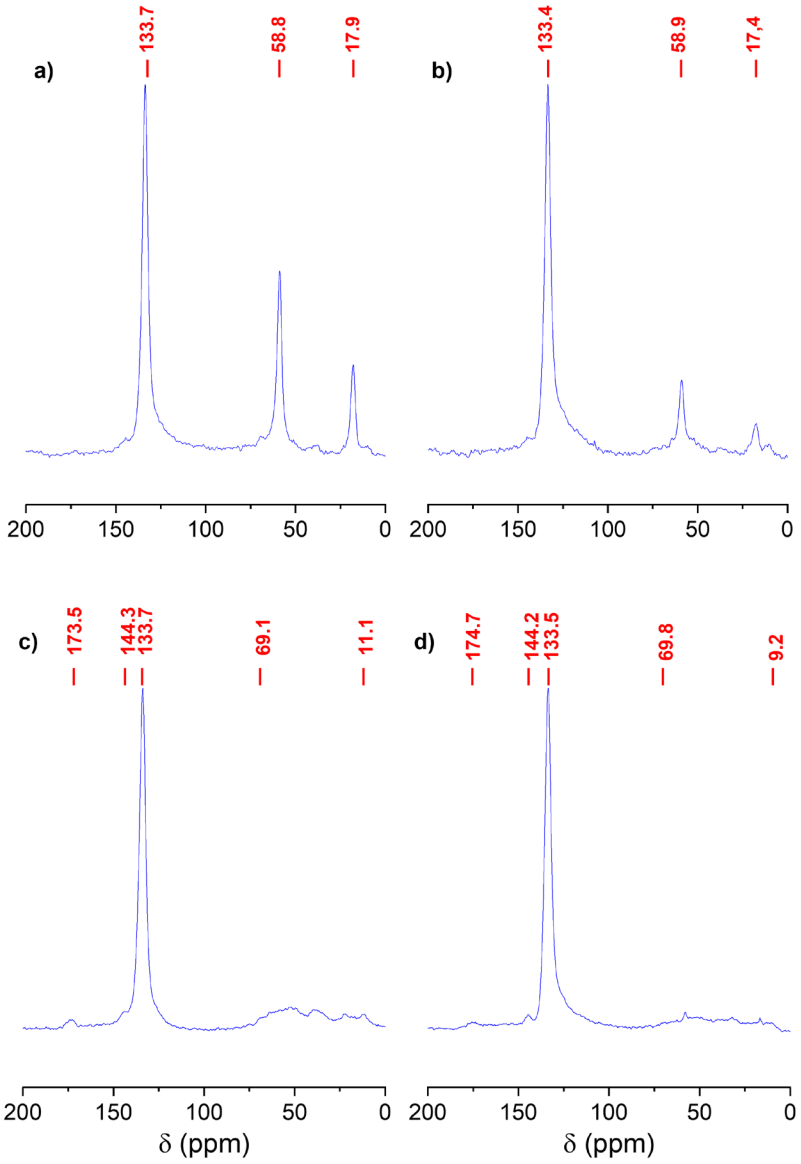

Figure S7. ^{13}C CP-MAS NMR spectra of the PAMAM-G0/BTEB gel a) before DTT treatment, b) after DTT treatment; of the PAMAM-G3/BTEB gel c) before DTT treatment, d) after DTT treatment

Figure S8 presents the fitted spectra of the materials prepared from pure PAMAM-G0-Si(OEt)$_3$ dendrimer before (**a**) and after (**b**) DTT treatment, respectively, while the corresponding integrated intensities are gathered in **Table S1**. The signal around -66 ppm corresponds to T^3 aliphatic silsesquioxanes, while that observed at -58 ppm arises from T^2 aliphatic silsesquioxanes. The extent of condensation appears high for both materials, with the T^3 signal being predominant. In addition, no cleavage of the Si-C bond occurred, with no Q^n signals being evident. It is interesting to note that T^1 species are observed after DTT treatment but not before. This observation, together with the increase in the abundance of T^2 sites compared with the T^3 sites, demonstrates that the DTT treatment cleaved the siloxane bonds to some extent. However, noting the intrinsic limitations of quantifying CP-MAS signal intensities, the extent of condensation (as indicated by the number of siloxane bonds) does not evolve significantly. Indeed, noting that each T^1 contributes 0.33 Si-O-Si groups to the Si-O-Si network; each T^2 contributes 0.67 and each T^3 contributes 1.0, the extent of condensation in the materials before and after treatment is 0.94 and 0.87, respectively.

Figure S9 and **Table S2** present the ^{29}Si NMR spectra and corresponding integrated intensities for the G3 PAMAM-derived dendrimer gels before and after DTT treatment. The data are similar to those observed for the G0 system, with T^3 silicon species predominating (signals at -65.6 and -65.7 ppm before and after DTT treatment, respectively) and no Si-C bond cleavage being observed. Before DTT treatment, T^1, T^2 and T^3 species were all identified, although the intensity of the T^1 signal was very weak. After DTT treatment no T^1 species were evident. The extent of condensation is 0.89 before DTT treatment and 0.91 after DTT treatment, indicating essentially no impact on the extent of condensation as a result of the DTT treatment.

The gels prepared from PAMAM-Si(OEt)$_3$ dendrimers and BTEB were analyzed in the same manner. The ^{29}Si solid state NMR spectrum of the PAMAM-G0-Si(OEt)$_3$ and BTEB gels (**Figure S10** and **Table S3**) exhibits several signals corresponding to the respective T^n sites of the aliphatic PAMAM- and aromatic BTEB-derived groups. In the case of the BTEB silicon sites, which are linked to an aromatic moiety, the chemical shifts move upfield with respect to those of the PAMAM silicon sites (all of which are linked to aliphatic moieties). A small quantity of Q^n silicon also appears for these samples due to some Si-C bond cleavage, presumably from the BTEB precursor where the Si-C_{sp2} bond is more susceptible to cleavage. Peak-fitting demonstrates that the six expected signals corresponding to the three aromatic and three aliphatic T^n silicon sites are present (**Table S3**). The chemical shifts were attributed according to those of pure PAMAM-G0-Si(OEt)$_3$-derived gel (**Table S1**) and pure BTEB-derived gel (T^1 = -62.0 ppm, T^2 = -70.5 ppm and T^3 = -78.7 ppm). In addition, as the quantity of Q^n silicon is nearly constant, it appears that the DTT treatment does not promote further Si-C cleavage. Here again, T^2 and T^3 species are predominant before and after cleavage, with the extent of condensation remaining essentially constant after DTT treatment (0.71 before cleavage; 0.73 after cleavage).

Similarly, the ^{29}Si NMR spectra of the gels prepared from PAMAM-G3-derived dendrimer and BTEB exhibited the signals expected for aliphatic and aromatic T^n silicon sites (**Figure S11** and **Table S4**), with no Q^n species being observed. As observed for the other gels, the extent of condensation (0.81 and 0.79 before and after treatment, respectively) is not impacted significantly by the DTT treatment.

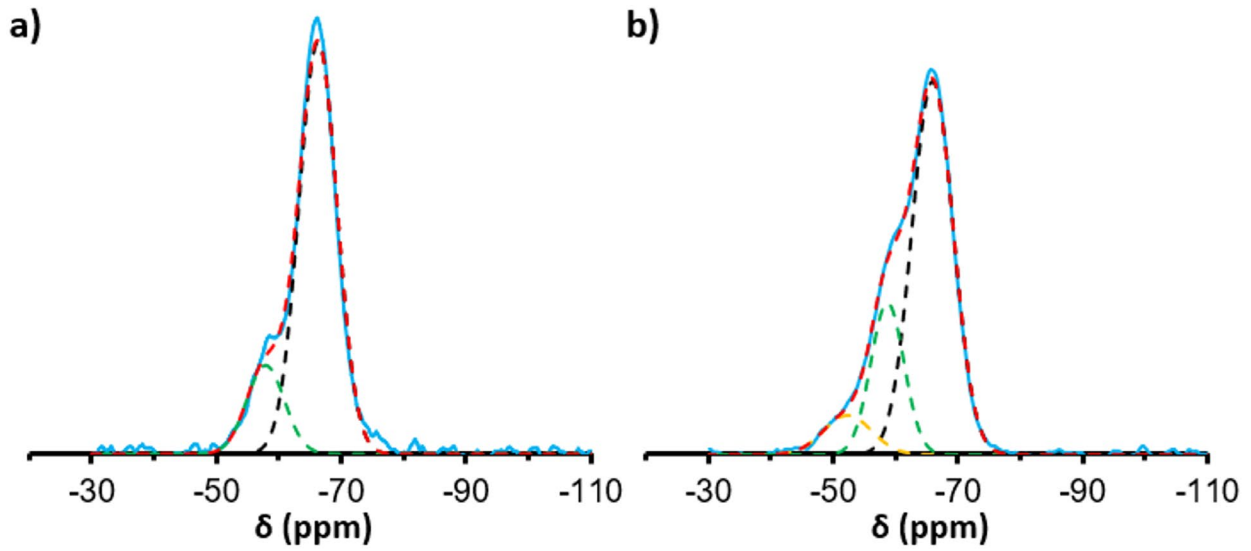

Figure S8. Signal fitting treatment of the ^{29}Si NMR spectra of the gels prepared from pure PAMAM-G0-Si(OEt)$_3$ a) before DTT treatment, b) after DTT treatment

Table S1. ^{29}Si solid state NMR spectra fitting of signal positions and proportions for the gel prepared from pure PAMAM-G0-Si(OEt)$_3$

	Silsesquioxane signal	Position (ppm)	Intensity (%)
PAMAM-G0 Gel	T^1	n.o.	n.o.
	T^2	-57.9	17.5
	T^3	-66.3	82.5
PAMAM-G0 Gel DTT cleaved	T^1	-51.8	8.5
	T^2	-58.8	22.5
	T^3	-66.0	69.0

n.o. = not observed

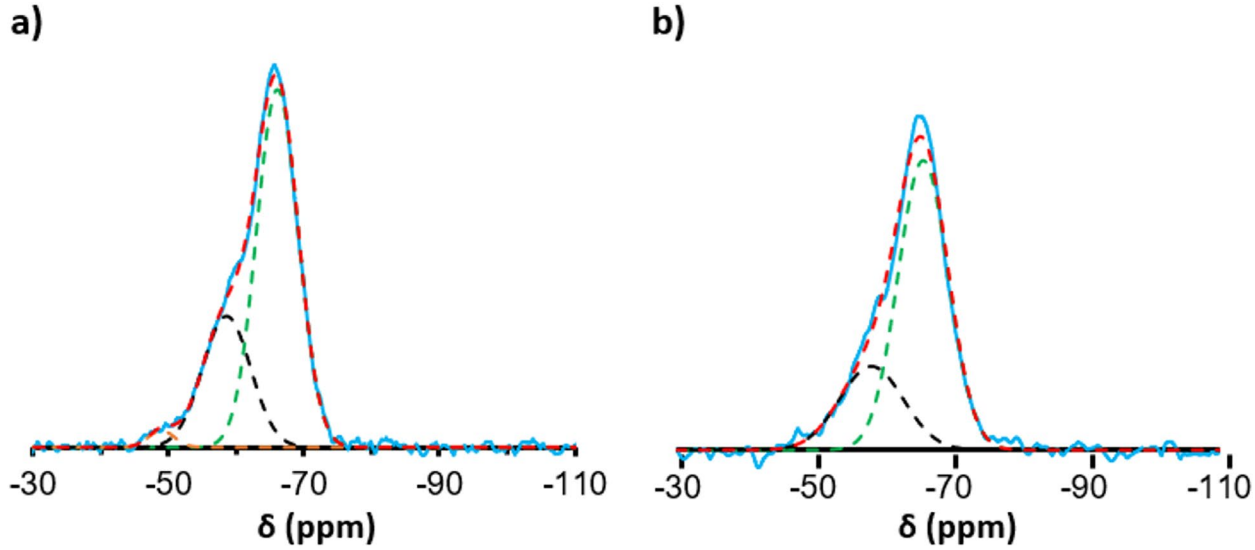

Figure S9. Signal fitting treatment of the ^{29}Si NMR spectra of the gels prepared from pure PAMAM-G3-Si(OEt)$_3$ a) before DTT treatment, b) after DTT treatment

Table S2. ^{29}Si solid state NMR spectra fitting of signal positions and proportions for the gel prepared from pure PAMAM-G3-Si(OEt)$_3$

	Silsesquioxane signal	Position (ppm)	Intensity (%)
PAMAM-G3 Gel	T^1	-49.0	2.0
	T^2	-58.6	29.1
	T^3	-66.1	68.9
PAMAM-G3 Gel DTT cleaved	T^1	n.o.	n.o.
	T^2	-58.7	26.8
	T^3	-66.0	73.2

n.o. = not observed

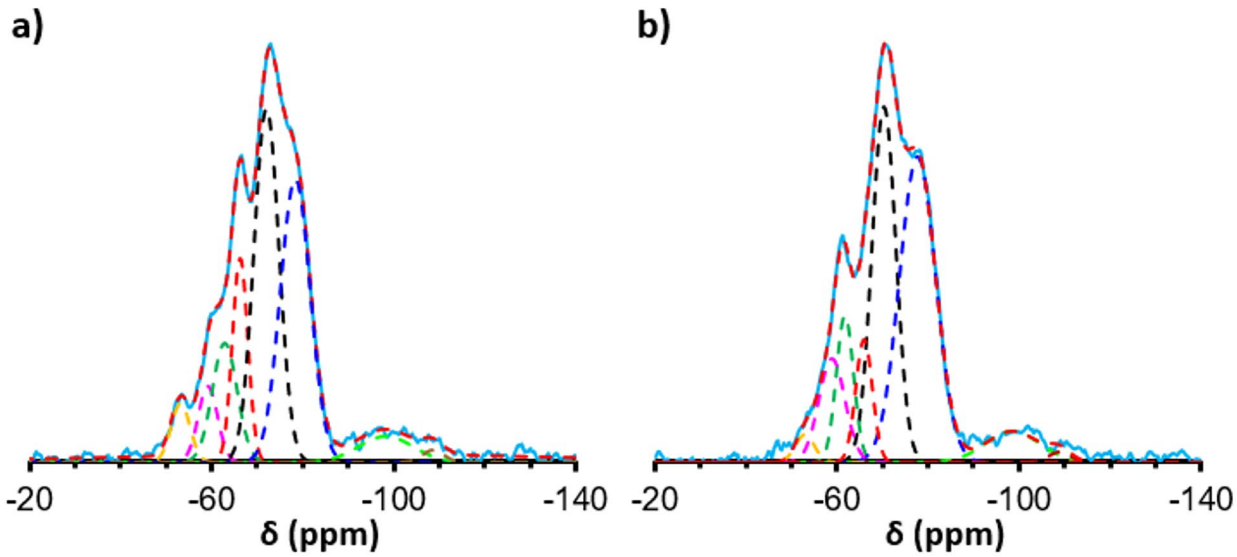

Figure S10. Signal fitting treatment of the ^{29}Si NMR spectra of PAMAM-G0/BTEB gels a) before DTT treatment, b) after DTT treatment

Table S3. ^{29}Si solid state NMR spectra fitting of signal positions and proportions for the PAMAM-G0/BTEB gel

	Precursor	**Silsesquioxane signal**	**Position (ppm)**	**Intensity (%)**
PAMAM-G0/BTEB Gel	PAMAM	T^1	-53.3	4.0
		T^2	-59.3	5.3
		T^3	-66.4	11.4
	BTEB	T^1	-63.0	10.7
		T^2	-72.2	32.1
		T^3	-78.5	30.7
		Q^n	-98.4 and -18.8	5.8
PAMAM-G0/BTEB Gel DTT cleaved	PAMAM	T^1	-52.8	1.8
		T^2	-58.7	9.2
		T^3	-65.8	7.0
	BTEB	T^1	-61.6	8.6
		T^2	-70.2	29.1
		T^3	-77.6	37.9
		Q^n	-98.4 and -108.8	6.5

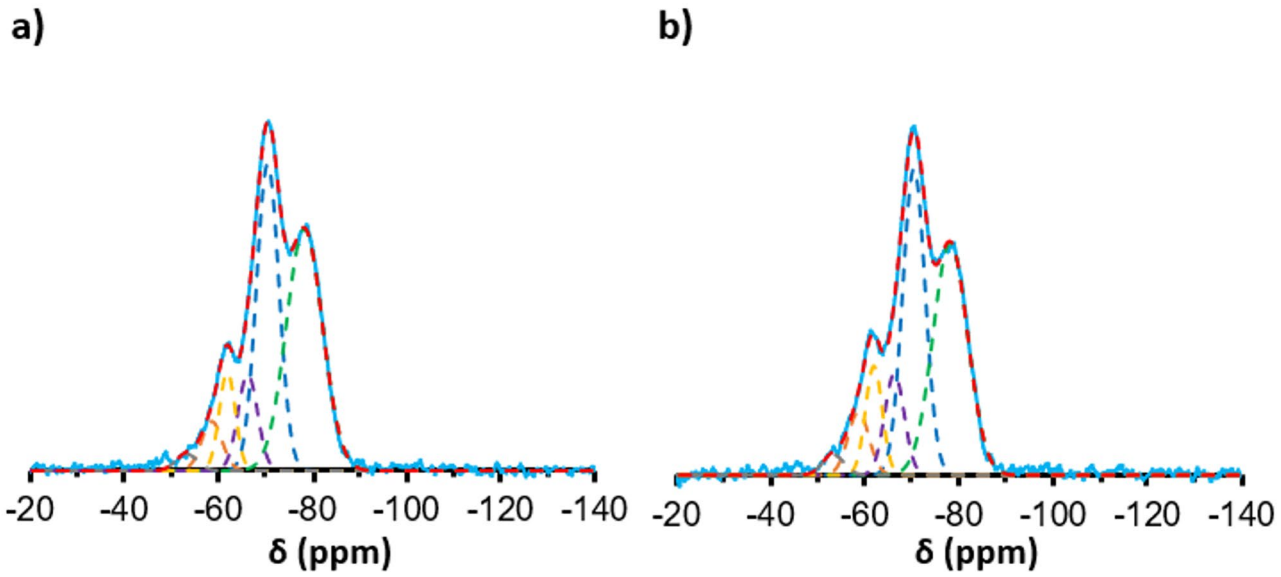

Figure S11. Signal fitting treatment of the ^{29}Si NMR spectra of PAMAM-G3/BTEB gels a) before DTT treatment, b) after DTT treatment

Table S4. ^{29}Si solid state NMR spectra fitting of signal positions and proportions for PAMAM-G3/BTEB gels

	Precursor	**Silsesquioxane signal**	**Position (ppm)**	**Intensity (%)**
PAMAM-G3/BTEB Gel	PAMAM	T^1	-53.3	1.7
		T^2	-58.6	5.0
		T^3	-66.3	9.2
	BTEB	T^1	-61.9	7.7
		T^2	-70.5	33.8
		T^3	-79.3	42.6
PAMAM-G3/BTEB Gel DTT cleaved	PAMAM	T^1	-53.3	2.1
		T^2	-58.6	6.5
		T^3	-66.3	9.7
	BTEB	T^1	-61.9	8.9
		T^2	-70.4	33.7
		T^3	-78.2	39.2

Chemical composition: infrared and Raman spectroscopy

A FTIR study was undertaken in order to identify the dominant bands of relevance to our system. Since a key moiety formed during cleavage of the dendrimer is the -SH group, the spectrum of DTT was recorded to identify the position of the SH stretching mode, which was observed at 2567 cm^{-1} as a weak band. In addition, as some of the gels were prepared with BTEB, its FTIR spectrum was recorded. The δ(C-H) mode is visible at 534 cm^{-1} as well as ν(C-H) at 3056 cm^{-1}. In the case of the PAMAM-G0-Si$(OEt)_3$ and BTEB, ν_{as}(Si-O-C) is visible at 1075-1077 cm^{-1}. The CH_3 antisymmetric and symmetric C-H stretching modes, together with the CH_2 antisymmetric stretching mode arising from the ethoxysilyl groups, can be seen at 2975, 2927 and 2887 cm^{-1}, respectively. In the case of the PAMAM-derived dendrimers, six precursors were analyzed by FTIR spectroscopy (**Figures S3 and S4**) to identify the key diagnostic bands:

- bis(hydroxyethyl)disulfide, a simple molecule and precursor of the synthesis of the linker.
- the linker to be grafted on the PAMAM.
- the linker-grafted PAMAM G0, bearing the terminal acetylenic function.
- the triethoxysilylated-grafted PAMAM G0 used in the synthesis of the materials.
- the linker-grafted PAMAM G3 bearing the terminal acetylenic function.
- the triethoxysilylated-grafted PAMAM G3 used in the synthesis of the materials.

The FTIR spectra (between 650 to 1900 cm^{-1}) of these precursors (**Figures S3** and **S4**) enable ν(C=O), between 1720 and 1734 cm^{-1}, to be identified. In addition, the PAMAM G0 and G3 dendrimers also exhibit the expected amide vibrations around 1650 and 1530 cm^{-1}. In the case of the PAMAM G0 and G3 Si$(OEt)_3$ dendrimers, the ethoxy vibrations are also visible around 1100 cm^{-1}. However, no signal related to the disulfide bond could be observed in the wavenumber range probed (450 to 4000 cm^{-1}).

Two model molecules, the DTT bearing thiol functions and bis(hydroxyethyl)disulfide used in the synthesis of the linker, were also studied via Raman spectroscopy to assign the bands arising from the disulfide and thiol moieties (**Figure 5, main text**). Indeed, as selection rules are different between FTIR and Raman spectroscopy, these bands could be observed via Raman but not infrared spectroscopy, reflecting the complementarity of the techniques for the characterizations of these groups. In the Raman spectrum of bis(hydroxyethyl)disulfide ν(S-S) at 512 cm^{-1} and ν(C-S) at 642 - 667 cm^{-1} can be readily identified. Other key bands can also be seen, including δ(C-C-S), δ(C-S-S) and ν(CH_2). In the dithiothreitol Raman spectrum, ν(C-S) at 738 cm^{-1}, δ(C-C-S) at 273 cm^{-1}, and ν(S-H) at 2569 cm^{-1} are clearly observed.

Table S5. Vibrations of the organic moieties of interest in the PAMAM dendrimer and BTEB precursors and their corresponding experimental values in the PAMAM-G0/G3 BTEB gels

Function	Band	Vibration mode	Theoretical band (cm^{-1})		Experimental band (cm^{-1})		Ref
			IR	Raman	IR	Raman	
Triazole	C-H	Sym. stretching	3000-2760				[11]
	C=C	Stretching	1531-1556 w	1531 s		1536/1533	[12-13]
	C-N	Stretching	1431	1447	1466/1462	1457/1457	[14]
		In plane ring stretching	1381 1442	1381		1343/-	[13]
	N=N C-N	Stretching	1208-1290 w	1290 s	1293/-	1292/1292	[11-12]
	C-H	In plane bending	1222	1230			[13]
		Ring breathing	1174	1184			[13]
	N=N	Stretching	1231 s	1231 m		1233/-	[12]
	C-N	Stretching	1085	1085			[12]
	N-N	Stretching	1010 w	1010 s		1028/1033	[12]
		In plane ring bending	949-955 974-995 s	949-950 985-995			[11-13]
		Out of plan ring bending	652-637 s	637			[11-12]
Disulfide	CS	Stretching	640-690 m	717-688 m 670-655 m		637/637	[15-16]
	SS	Stretching	500-510 w	505-502 s		510/513	[15-16]
	CCS	Scissoring	435-440 w 420-400 m	440-434 418-417 m		393/391	[16]
	CSS	Scissoring		327-310 m 306-295 m			[16]

Function	Band	Vibration mode	Theoretical band (cm^{-1})		Experimental band (cm^{-1})		Ref
			IR	**Raman**	**IR**	**Raman**	
Thiol	SH	Stretching	2525/2497	2573		2572*	[17]
	SH	Bending	984-978	972			[17]
	CS	Stretching	727-725	726			[15, 17]
	CCS	Bending	300-297	288			[17]
	SH	Torsional		244			[17]
PAMAM	N-H	Stretching	3330-2372 s				[18-19]
	CH_2	Asym. Stretching	2943-2940 s 2907 m 2868 w	2910	2933/2933	2929/2925	[19-20]
	CH_2	Sym. Stretching	2850-2820 m	2820 2855	2868/2867	2868/2875	[18-20]
	C=O C-N-H (Amide II)	Stretching & bending	1551 s		1548/1544		[18]
	C=O C-N-H (Amide I)	Stretching & bending	1651-1620 s	1690-1630	1653/1646		[18-19, 21]
Ester	C=O	Stretching			1736/1729		
Aromatic ring	C-H	Stretching	3067	3068-2818	3061/3073	3043/3045	[22-23]
	C=C	Stretching	1590	1590		1599/1599	[22-23]
		Ring breathing		977			[23]
		In plane ring deformation		671 634	662/645	637/637	[24]
		Out of plane ring deformation	524		528/-		[24]

Function	Band	Vibration mode	Theoretical band (cm^{-1})		Experimental band (cm^{-1})		Ref
			IR	Raman	IR	Raman	
Ethoxysilane	CH_3	Asym. Stretching	2985-2976 m	2979 s	2978/2971	2974/2960	[25]
	CH_2	Asym. Stretching	2931-2928 w	2940-2930 s	2933/2933	2929/2925	[25]
	CH_3	Sym. Stretching	2897-2887 w	2889 s	2897/2885	2888/2887	[25]
	CH_2	Sym. Stretching	2854-2850m	2875 m	2868/2867	2868/2875	[25]
Silsesquioxane	Si-OH	Stretching	3445		3413/3337		[25]
	Si-O-Si	Symmetric Stretching	1160-830 s	830-826 w	1142-1013 /1192-1013		[25-26] [22]
	Si-C	Stretching	1198	1120		1106/1106	[22-23]

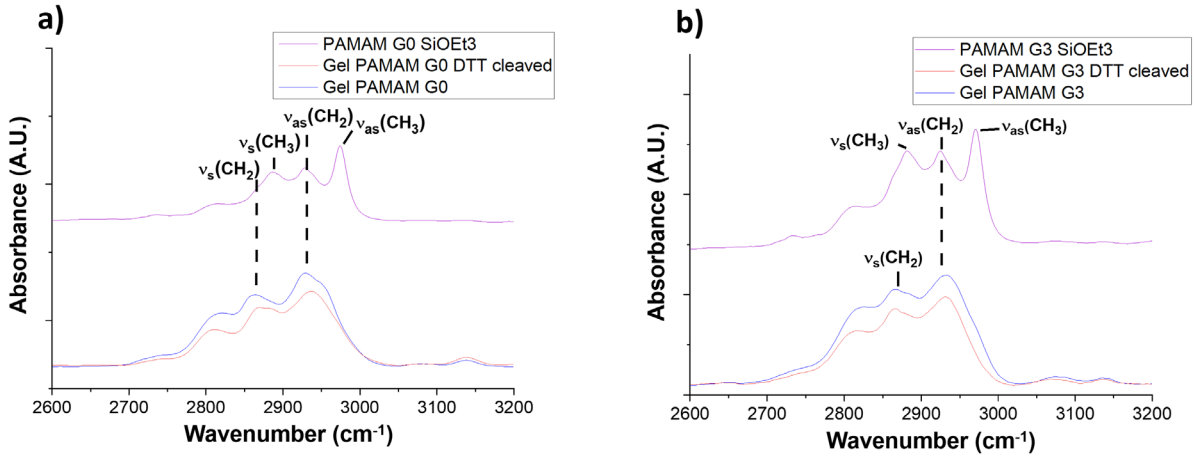

Figure S12. FTIR spectra, normalized against ν(Si-O-Si), before and after DTT cleavage in the range 2600 to 3200 cm^{-1} for a) PAMAM-G0 gel b) PAMAM-G3 gel. ν: stretching mode

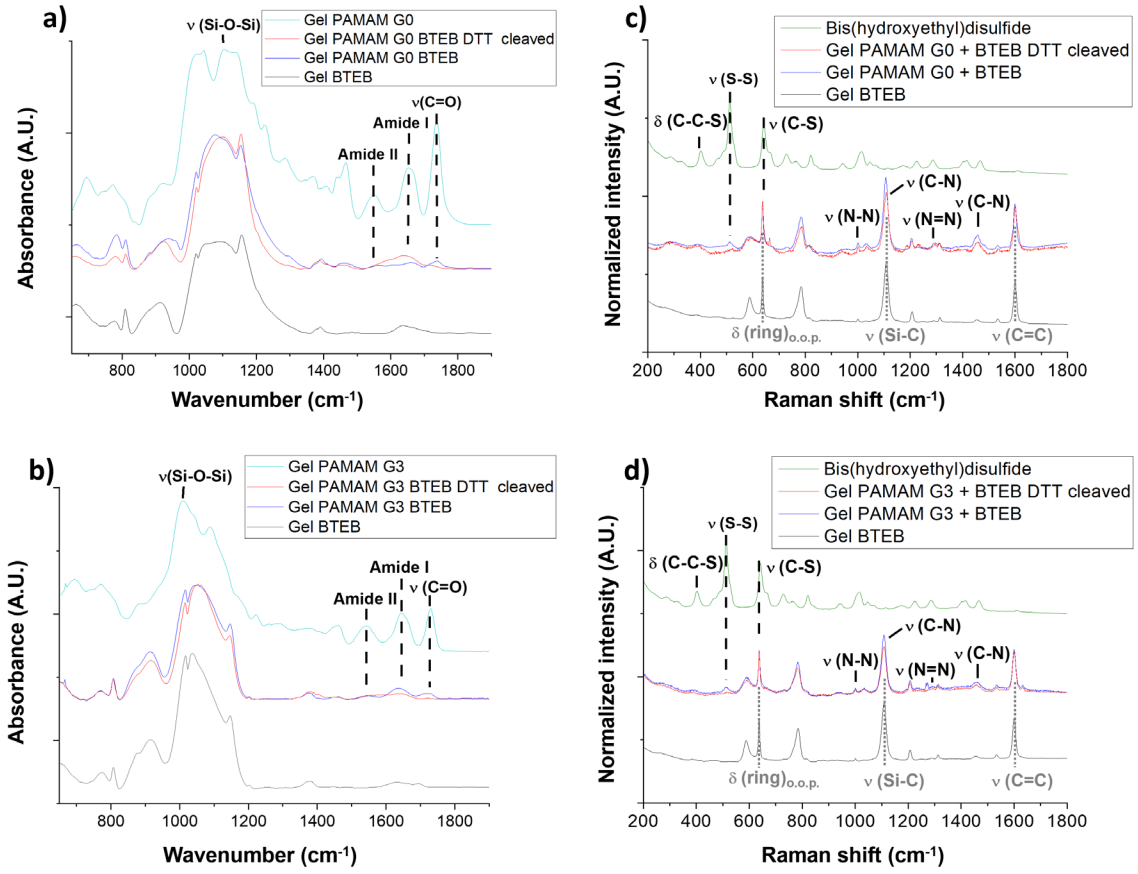

Figure S13. FTIR spectra, normalized against ν(Si-O-Si), before and after DTT cleavage in the range 650 to 1900 cm^{-1} for a) PAMAM-G0/BTEB gel b) PAMAM-G3/BTEB gel; Raman spectra, normalized against ν(N-N), before and after DTT cleavage in the range 200 - 1800 cm^{-1} c) PAMAM-G0/BTEB gel d) PAMAM-G3/BTEB gel. ν: stretching, δ: scissoring modes

Textural properties: pore size distributions from N_2 physisorption isotherms

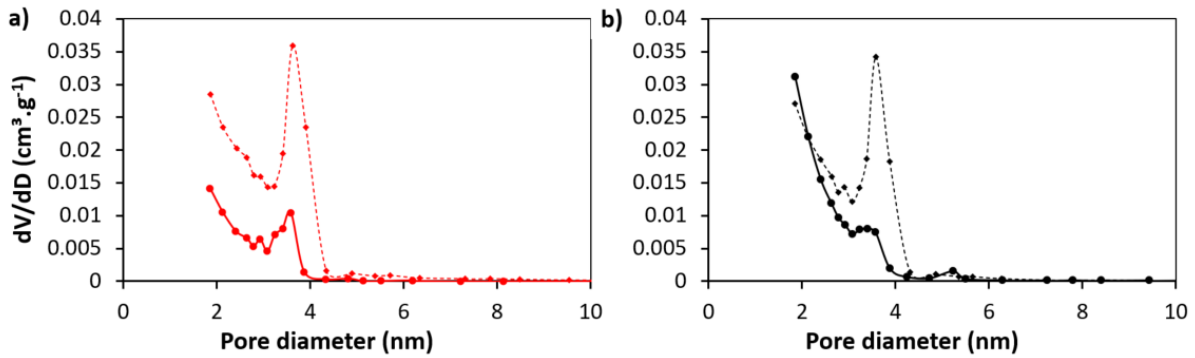

Figure S14. BJH pore size distribution of (a) PAMAM-G0/BTEB gel (red); and (b) PAMAM-G3/BTEB gel (black). Solid lines, before DTT cleavage; dashed lines, after DTT cleavage

Thermal Analysis of PAMAM Gels

Thermogravimetric analysis offers additional insights into the composition and properties of the gels, and variations in the mass of the PAMAM-G3 and PAMAM-G3/BTEB gels before and after DTT cleavage are illustrated in **Figure S15**. The PAMAM-G3 gel (**Figure S15(a)**, blue curves) exhibits only negligible mass loss at temperatures less than 200 ºC (< 4 %), consistent with the presence of only small quantities of water within the pores. At higher temperatures, a complex series of mass loss events is evident, with well-defined peaks observed in the dTGA plots at 220-225, 330-335 and ~600 ºC, corresponding to mass losses of ~19, 22 and 40 %, respectively, associated with decomposition of the dendrimer. The residual SiO_2 mass was around 19 % at 650 ºC, which is comparable to the theoretical value of 19.2 %. Previous TGA studies of PAMAM dendrimer systems have revealed that decomposition of the dendrimer skeleton via a retro-Michael reaction is complete by 500 ºC under oxidising conditions and in the presence of metal species.[27-28]

DTT cleavage of the dendrimer core leads to substantial changes in the observed TGA and dTGA plots (**Figure S15(a)**, red curves). The onset of significant mass loss begins at lower temperatures, with dTGA peaks observed at 195-200, ~290 and 565-570 ºC corresponding to mass losses of ~11, 45 and 33 %, respectively. The lower onset temperature for decomposition presumably arises from the increased porosity of the DTT-cleaved sample and enhanced ingress of air. Partial or complete loss of the dendrimer core via DTT cleavage would also be expected to result in an increase in the residual inorganic content following oxidative decomposition of the dendrimer. However, the data in **Figure S15(a)** indicate that the converse is true, with a significant reduction in the mass of SiO_2 retained after decomposition of the dendrimer skeleton being evident at temperatures exceeding 580 ºC. The ^{29}Si NMR and FTIR data discussed above demonstrate that DTT treatment has essentially no impact on the structure of the silsesquioxane backbone of the nanocomposite, suggesting that no T^1, T^2 or T^3 silsesquioxane species are lost in solution during cleavage of the dendrimer core. Hence, the loss of a significant fraction of the inorganic silsesquioxane component at high temperatures is tentatively attributed to the formation of volatile oligomeric and/or cyclic monomeric siloxane species at high temperatures, as described by Huang *et al*.[29]

The thermal decomposition of PAMAM-G3/BTEB, illustrated in **Figure S15(b)**, is dominated by oxidation of the dominant BTEB-derived silsesquioxane component, with only minor differences being observed before and after DTT cleavage of the dendrimer core. The residual mass following decomposition of the dendrimer skeleton is around 41 % for the as-

prepared and DTT-cleaved samples, which is lower than the expected values of 50 and 57 %, respectively, due to the presence of T^1 and T^2 siloxane species in both cases and incomplete cleavage of the core in the latter case.

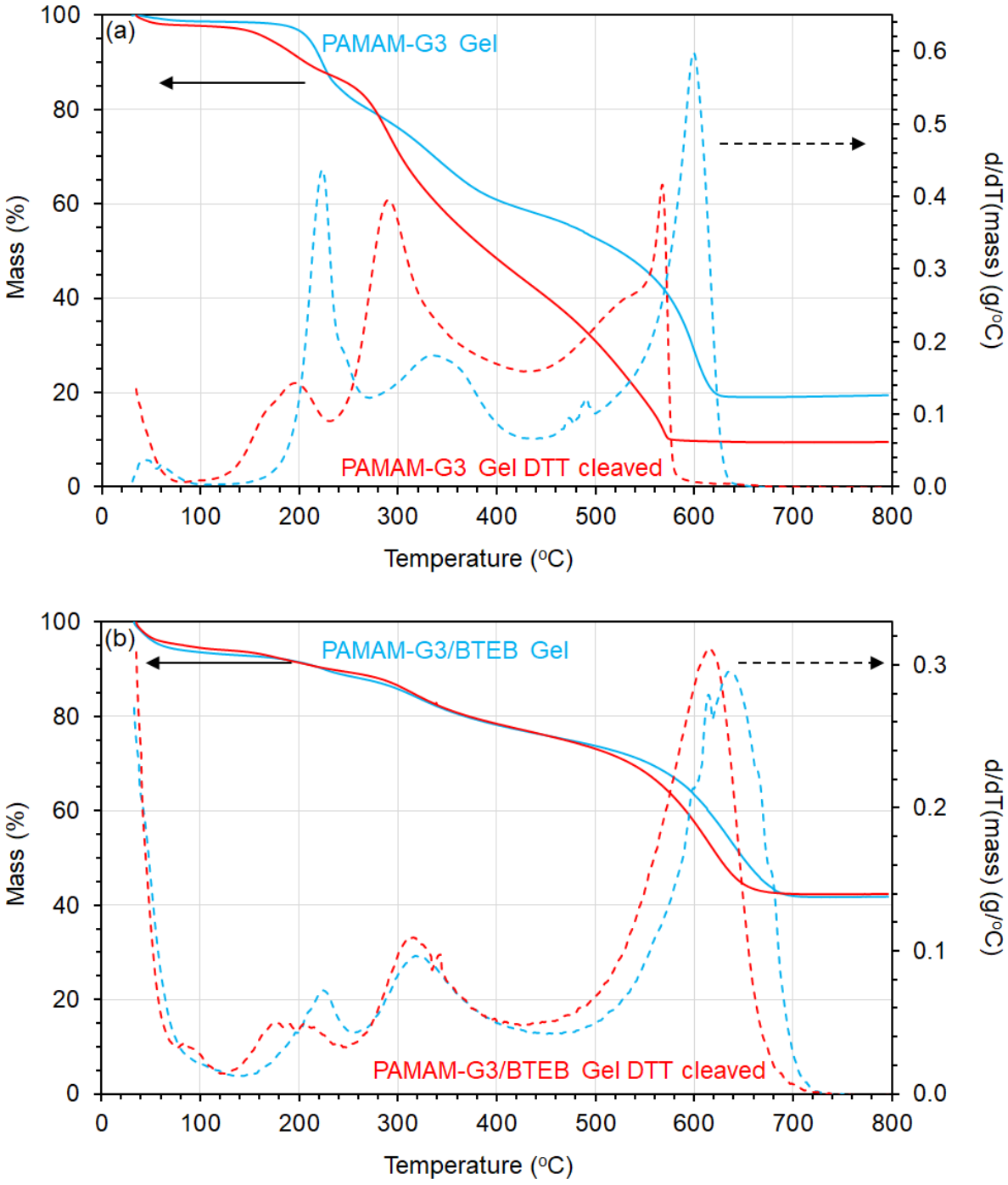

Figure S15. TGA (solid lines) and dTGA plots (dashed lines) for (a) PAMAM-G3 and (b) PAMAM-G3/BTEB gels before and after DTT cleavage

Representative EDX Elemental Maps and EDX Spectra of PAMAM-G0/BTEB, PAMAM-G3/BTEB and Pure BTEB Gels

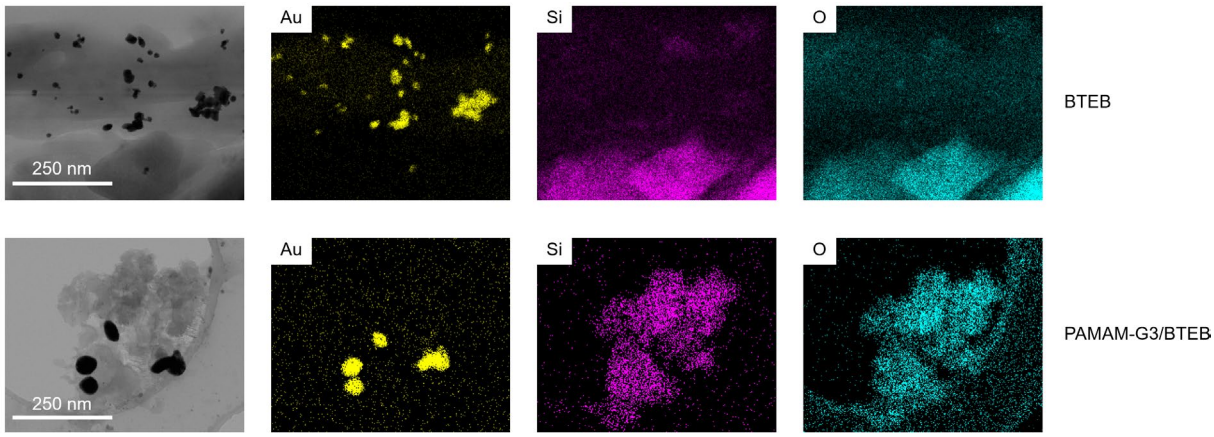

Figure S16. Representative EDX elemental maps of Au, Si and O in pure BTEB (top row) and PAMAM-G3/BTEB gels (bottom row). Size bar, 250 nm

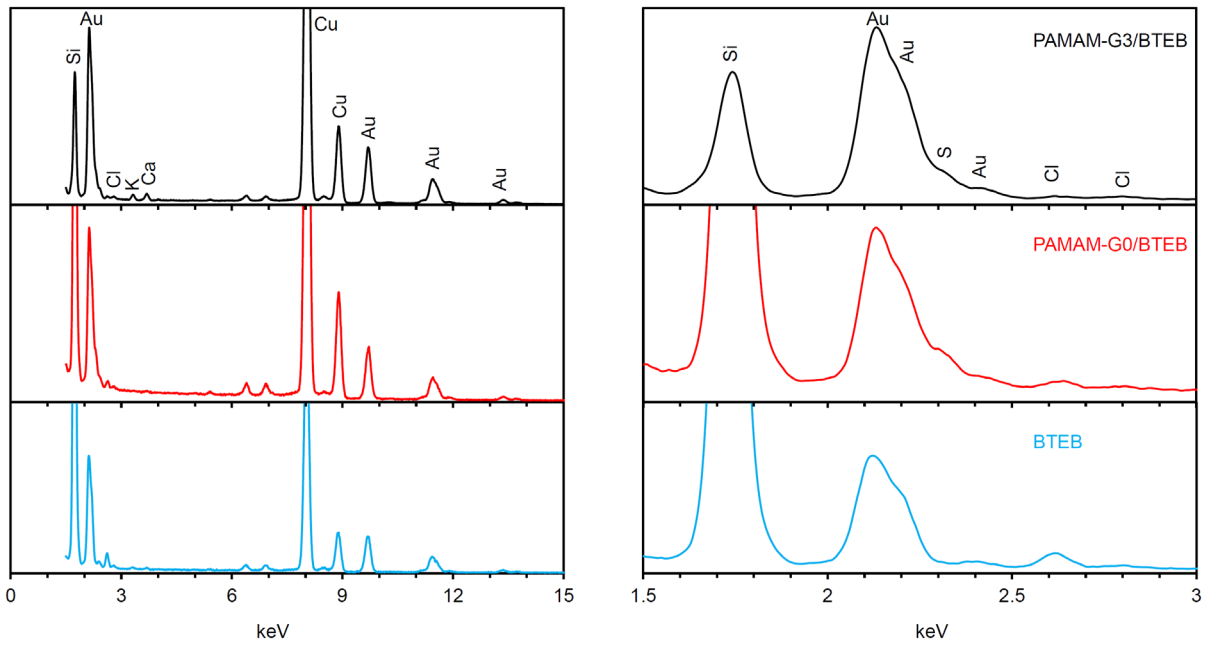

Figure S17. Representative EDX spectra (1.5 to 15 keV) of PAMAM-G3/BTEB (black), PAMAM-G0/BTEB (red) and pure BTEB gels (blue). Right: Expanded view (1.5 to 3.0 keV)

Estimating the S:Si atomic ratio from weighted subtraction of the reconstructed Au spectrum

The EDX spectrum of the Au-impregnated BTEB gel (**Figure S18**) can be well fitted with the expected peaks arising from Si and Au, together with minor quantities of Cl (retained after

impregnation with $NaAuCl_4$). From these data, the spectrum of Au can be reconstructed by simple co-addition of the four Gaussian profiles arising from Au in this region of the EDX spectrum at 1.64, 2.13, 2.22 and 2.40 keV (see inset to **Figure S18**). The corresponding EDX spectrum of the impregnated PAMAM-G3/BTEB gel, **Figures S19 and S20**, exhibits all of the peaks observed in the impregnated BTEB gel, together with an additional peak arising from sulfur at 2.30 keV.

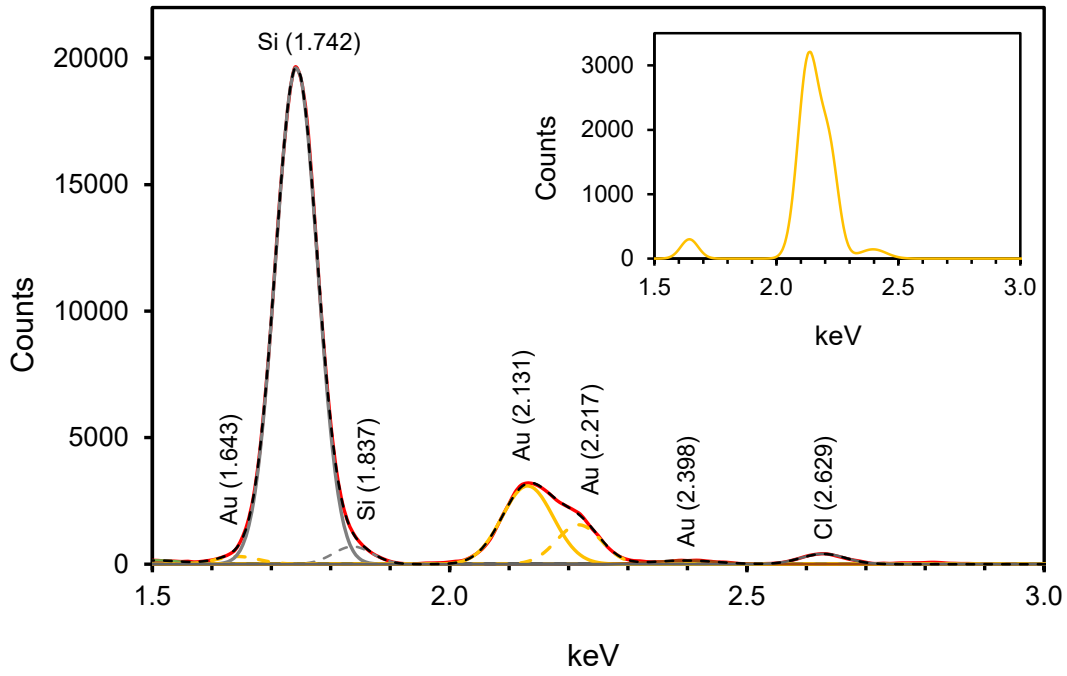

Figure S18. Curve fitting analysis of the EDX spectrum of Au-impregnated BTEB gel. Inset: the reconstructed Au spectrum

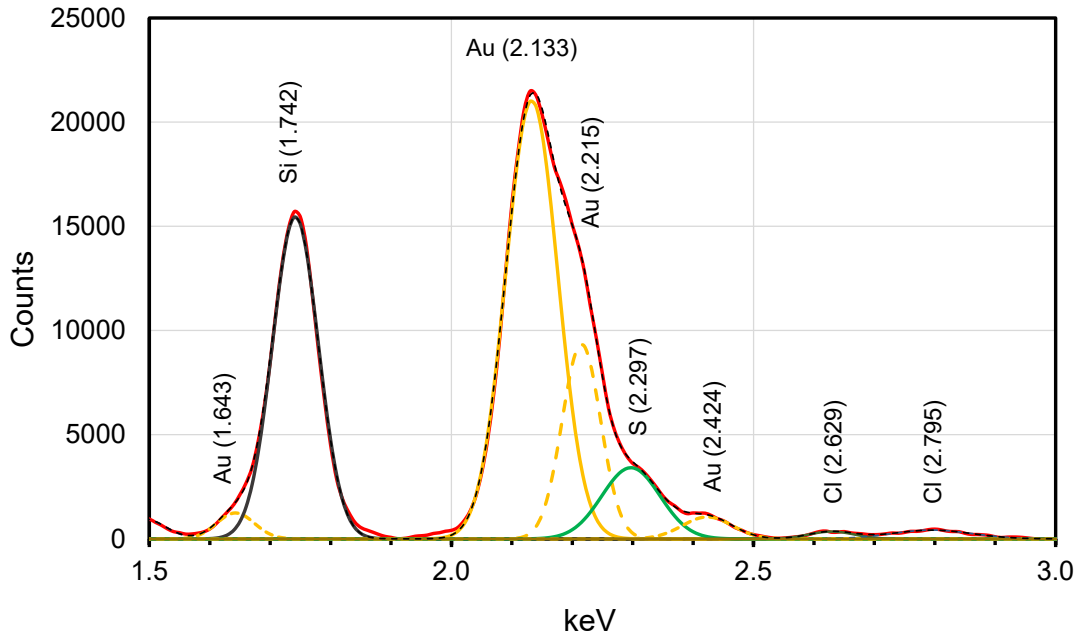

Figure S19. Curve fitting analysis of the EDX spectrum of Au-impregnated PAMAM-G3/BTEB gel

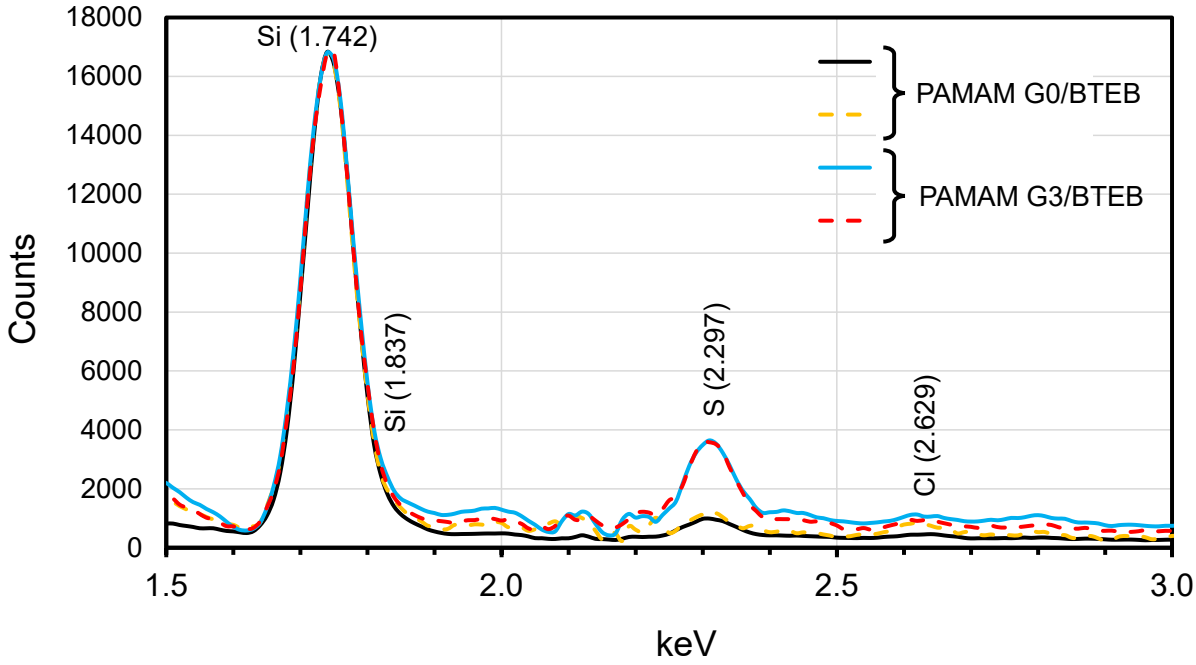

Figure S20. Weighted difference spectra obtained by subtracting the gold spectrum synthesized from analysis of the Au-impregnated BTEB gel from the spectra of the Au-impregnated PAMAM-G0/BTEB and PAMAM-G3/BTEB gel. The procedure was repeated for spectra acquired from two different regions of each sample. The difference spectra have been normalized to the intensity of the Si peak at 1.74 keV

S3.3 PMO Synthesis and inner dendrimer cleavage

Scoping studies to optimize synthesis of PAMAM/BTEB PMOs

Tests were performed using the G0 dendrimer. A mixture of PAMAM-G0-Si(OEt)$_3$ and BTEB was thus prepared, which was then added to a surfactant solution. It was noted that solvent trapped in the dendrimer strongly affected the pre-formed surfactant mesophase during the addition step. Hence, a careful procedure was implemented to remove the solvent. The dried, nearly-solvent-free precursor mixture was then used to produce materials via sol-gel processing, in the presence of a SDA. Although the acidic or basic conditions used for the PMO synthesis can possibly cleave the ester of the PAMAM-G0-Si(OEt)$_3$, experiments under basic, neutral, and acidic conditions were performed. Organized pore networks could only be observed under acidic conditions. These latter conditions take advantage of the use of a neutral block copolymer, which is expected to interfere to a lesser extent with the PAMAM amine and amide functions than cationic surfactants. In addition, block copolymer micelles are neutral and generally larger than those obtained with cationic surfactants. The micelle should thus be less impacted by the presence of the dendrimer. In order to increase the prospects of obtaining an organized structure, the quantity of BTEB used in the synthesis was increased (PAMAM-G0-Si(OEt)$_3$/BTEB = 1/384).

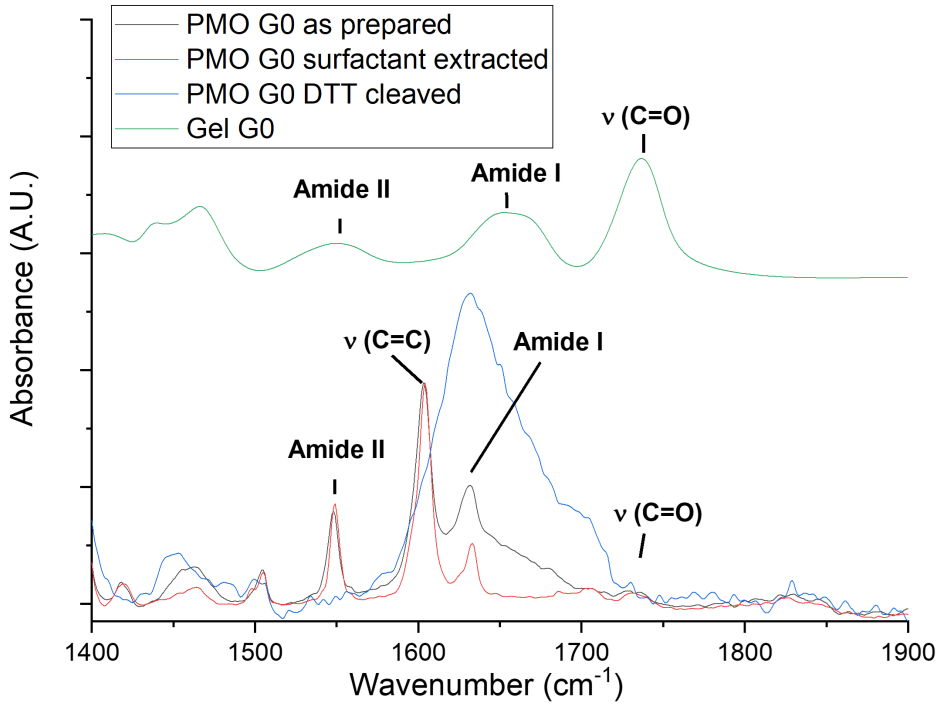

Figure S21. Synthetic pathway to PMOs with bimodal porosity and pendant functions. Where feasible, intensities were normalized against the C=C stretching mode at 1604 cm^{-1}. Note that it was not possible to remove water from the sample after DTT cleavage, even under reduced pressure for several days

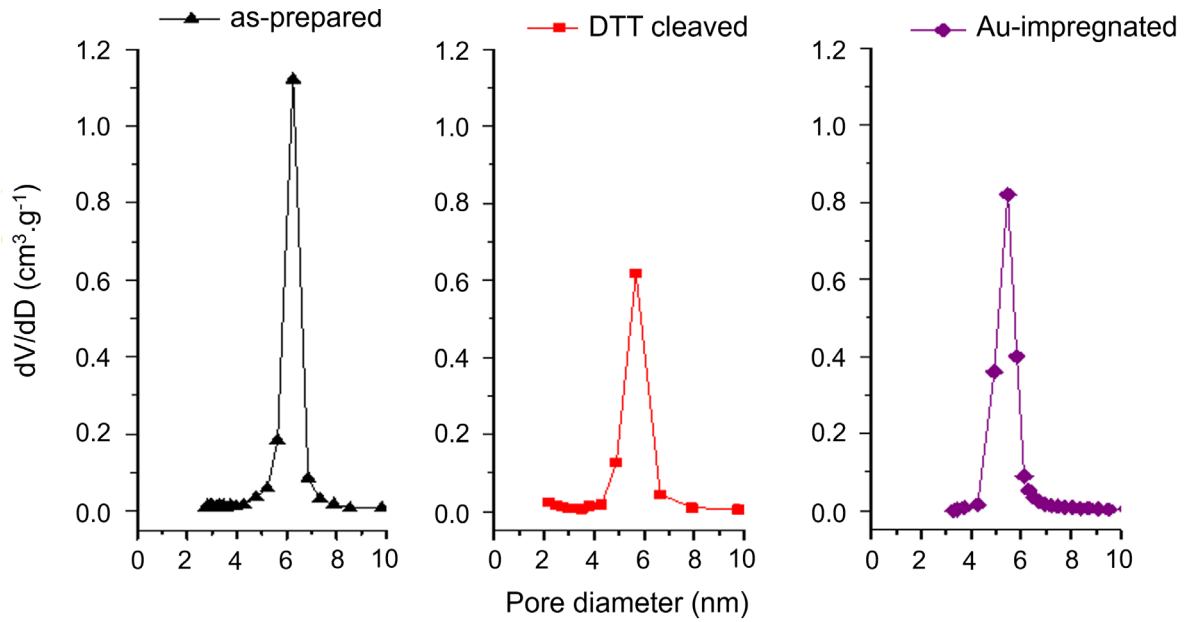

Figure S22. BJH pore size distribution of PAMAM-G0/BTEB PMO prior to surfactant extraction (black); after surfactant extraction and DTT cleavage (red); and after gold impregnation (purple)

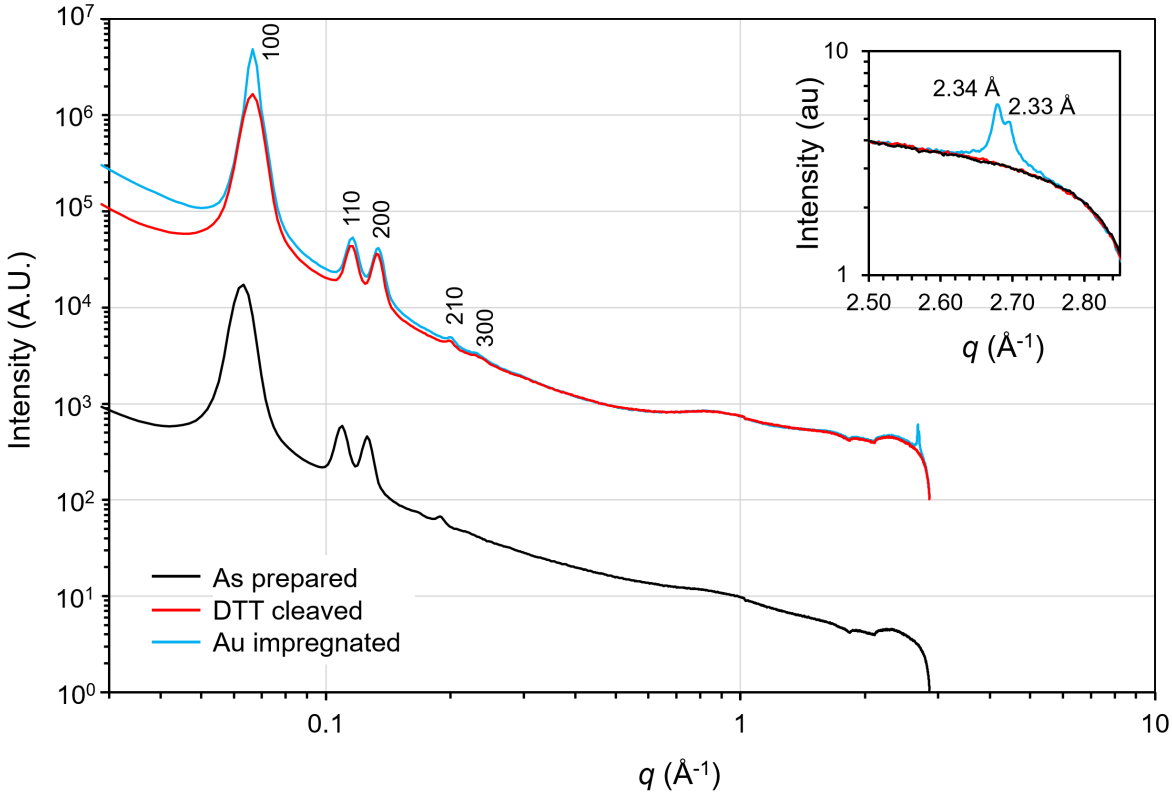

Figure S23. SWAXS patterns of the PAMAM-G0/BTEB PMO as-prepared (black); after DTT cleavage (red); and after Au-impregnation (blue). Note that the red curve has been offset to demonstrate the enhanced electronic contrast of the 2D-hexagonal PMO scattering after Au impregnation

References

[1] X. Liu, W. Shao, Y. Zheng, C. Yao, L. Peng, D. Zhang, X. Y. Hu, L. Wang, *Chem. Commun.* **2017**, 53, 8596.

[2] L. Li, X. Wang, J. Yang, X. Ye, C. Wu, *Macromolecules* **2014**, 47, 650.

[3] V. Weiss, C. Argyo, A. A. Torrano, C. Strobel, S. A. Mackowiak, A. Schmidt, S. Datz, T. Gatzenmeier, I. Hilger, C. Bräuchle, T. Bein, *Microporous Mesoporous Mater.* **2016**, 227, 242.

[4] S. Shenoi-Perdoor, A. Noureddine, F. Dubois, M. Wong Chi Man, X. Cattoën, in *Handbook of Sol-Gel Science and Technology: Processing, Characterization and Applications*, DOI: 10.1007/978-3-319-32101-1_95, Springer International Publishing **2018**, p. 3001.

[5] L. Balogh, A. De Leuze-Jallouli, P. Dvornic, Y. Kunugi, A. Blumstein, D. A. Tomalia, *Macromolecules* **1999**, 32, 1036.

[6] K. Bürglová, A. Noureddine, J. Hodačová, G. Toquer, X. Cattoën, M. Wong Chi Man, *Chem. Eur. J.* **2014**, 20, 10371.

[7] D. Kumar, V. B. Reddy, R. S. Varma, *Tetrahedron Lett.* **2009**, 50, 2065.

[8] M. I. Montañez, F. Najera, E. Perez-Inestrosa, *Polym.* **2011**, 3, 1533.

[9] F. D. Zhang, Y. Liu, J. C. Xu, S. J. Li, X. N. Wang, Y. Sun, X. L. Zhao, *Adv. Manuf.* **2015**, 3, 221.

[10] A. W. Bosman, H. M. Janssen, E. W. Meijer, *Chem. Rev.* **1999**, 99, 1665.

[11] S. G. Aziz, S. A. Elroby, A. Alyoubi, O. I. Osman, R. Hilal, *J. Mol. Model.* **2014**, 20, 1.

[12] A. A. Jbarah, K. Banert, R. Holze, *Vib. Spectrosc.* **2007**, 44, 142.

[13] A. A. Jbarah, A. Ihle, K. Banert, R. Holze, *Journal of Raman Spectroscopy* **2006**, 37, 123.

[14] H. Malarkodi, M. Saminathan, R. Ezhilarasi, D. Murugan, A. Ponnuswamy, *ChemistrySelect* **2018**, 3, 11552.

[15] D. W. Scott, J. P. McCullough, *J. Am. Chem. Soc.* **1958**, 80, 3554.

[16] H. Ramsis, M. Selkti, J. Roger, J. L. Delarbre, A. Tomas, L. Maury, A. Ennaciri, *J. Raman Spectrosc.* **2001**, 32, 125.

[17] J. R. Durig, J. J. Klaassen, B. S. Deodhar, T. K. Gounev, A. R. Conrad, M. J. Tubergen, *Spectrochim. Acta Part A Mol. Biomol. Spectrosc.* **2012**, 87, 214.

[18] A. Manna, T. Imae, K. Aoi, M. Okada, T. Yogo, *Chem. Mater.* **2001**, 13, 1674.

[19] P. M. R. Paulo, *J Chem Phys* **2010**, 132.

[20] A. P. Davis, G. Ma, H. C. Allen, *Anal. Chim. Acta* **2003**, 496, 117.

[21] G. Socrates, *Infrared and Raman Characteristic Group Frequencies: Tables and Charts, 3rd Edition*, John Wiley and Sons, **2004**.

[22] J. Croissant, X. Cattoën, M. Wong Chi Man, P. Dieudonné, C. Charnay, L. Raehm, J. O. Durand, *Adv Mater* **2015**, 27, 145.

[23] V. Rebbin, M. Jakubowski, S. Pötz, M. Fröba, in *Studies in Surface Science and Catalysis*, Vol. 154 A, 2004, 568.

[24] F. Hoffmann, M. Güngerich, P. J. Klar, M. Fröba, *J. Phys. Chem. C* **2007**, 111, 5648.

[25] Y. S. Li, A. Ba, *Spectrochim. Acta Part A Mol. Biomol. Spectrosc.* **2008**, 70, 1013.

[26] G. Creff, G. Arrachart, P. Hermet, H. Wadepohl, R. Almairac, D. Maurin, J. L. Sauvajol, C. Carcel, J. J. E. Moreau, P. Dieudonné, M. Wong Chi Man, J. L. Bantignies, *Phys. Chem. Chem. Phys.* **2012**, 14, 5672.

[27] O. Ozturk, T. J. Black, K. Perrine, K. Pizzolato, C. T. Williams, F. W. Parsons, J. S. Ratliff, J. Gao, C. J. Murphy, H. Xie, H. J. Ploehn, D. A. Chen, *Langmuir* **2005**, 21, 3998.

[28] S. Ghosh, A. H. Khan, S. Acharya, *J. Phys. Chem. C* **2012**, 116, 6022.

[29] Y. Huang, J. Yan, D. Wang, S. Feng, C. Zhou, *Polym.* **2021**, 13.